**Atmospheric
Chemistry
and Physics**

Trends and variations in CO, C_2H_6, and HCN in the Southern Hemisphere point to the declining anthropogenic emissions of CO and C_2H_6

G. Zeng[1], S. W. Wood[1,*], O. Morgenstern[1], N. B. Jones[2], J. Robinson[1], and D. Smale[1]

[1]National Institute of Water and Atmospheric Research, Lauder, New Zealand
[2]School of Chemistry, University of Wollongong, Wollongong, New South Wales, Australia
[*]now at: 1981 Omakau-Chatto Creek Road, Alexandra, New Zealand

Correspondence to: G. Zeng (guang.zeng@niwa.co.nz)

Abstract. We analyse the carbon monoxide (CO), ethane (C_2H_6) and hydrogen cyanide (HCN) partial columns (from the ground to 12 km) derived from measurements by ground-based solar Fourier Transform Spectroscopy at Lauder, New Zealand (45° S, 170° E), and at Arrival Heights, Antarctica (78° S, 167° E), from 1997 to 2009. Significant negative trends are calculated for all species at both locations, based on the daily-mean observed time series, namely CO $(-0.94 \pm 0.47 \% \, yr^{-1})$, C_2H_6 $(-2.37 \pm 1.18 \% \, yr^{-1})$ and HCN $(-0.93 \pm 0.47 \% \, yr^{-1})$ at Lauder and CO $(-0.92 \pm 0.46 \% \, yr^{-1})$, C_2H_6 $(-2.82 \pm 1.37 \% \, yr^{-1})$ and HCN $(-1.41 \pm 0.71 \% \, yr^{-1})$ at Arrival Heights. The uncertainties reflect the 95 % confidence limits. However, the magnitudes of the trends are influenced by the anomaly associated with the 1997–1998 El Niño Southern Oscillation event at the beginning of the time series reported. We calculate trends for each month from 1997 to 2009 and find negative trends for all months. The largest monthly trends of CO and C_2H_6 at Lauder, and to a lesser degree at Arrival Heights, occur during austral spring during the Southern Hemisphere tropical and subtropical biomass burning period. For HCN, the largest monthly trends occur in July and August at Lauder and around November at Arrival Heights. The correlations between CO and C_2H_6 and between CO and HCN at Lauder in September to November, when the biomass burning maximizes, are significantly larger that those in other seasons. A tropospheric chemistry-climate model is used to simulate CO, C_2H_6, and HCN partial columns for the period of 1997–2009, using interannually varying biomass burning emissions from GFED3 and annually periodic but seasonally varying

emissions from both biogenic and anthropogenic sources. The model-simulated partial columns of these species compare well with the measured partial columns and the model accurately reproduces seasonal cycles of all three species at both locations. However, while the model satisfactorily captures both the seasonality and trends in HCN, it is not able to reproduce the negative trends in either C_2H_6 or CO. A further simulation assuming a 35 % decline of C_2H_6 and a 26 % decline of CO emissions from the industrial sources from 1997 to 2009 largely captures the observed trends of C_2H_6 and CO partial columns at both locations. Here we attribute trends in HCN exclusively to changes in biomass burning and thereby isolate the influence of anthropogenic emissions as responsible for the long-term decline in CO and C_2H_6. This analysis shows that biomass burning emissions are the main factors in controlling the interannual and seasonal variations of these species. We also demonstrate contributions of biomass burning emission from different southern tropical and sub-tropical regions to seasonal and interannual variations of CO at Lauder; it shows that long-range transport of biomass burning emissions from southern Africa and South America have consistently larger year-to-year contributions to the background seasonality of CO at Lauder than those from other regions (e.g. Australia and South-East Asia). However, large interannual anomalies are triggered by variations in biomass burning emissions associated with large-scale El Niño Southern Oscillation and prolonged biomass burning events, e.g. the Australian bush fires.

1 Introduction

In the mid- and high latitudes of the Southern Hemisphere (SH), measurements of trace gases are sparse. Mid-infrared solar Fourier Transform Spectroscopy (FTIR) measurements made by the National Institute of Water and Atmospheric Research at Lauder (45° S, 170° E, 370 m a.m.s.l.) and Arrival Heights (78° S, 167° E, 220 m a.m.s.l.) constitute two of the most comprehensive multi-year time series of trace gases in the SH (http://www.ndsc.ncep.noaa.gov/). Measured species include not only those of significance to stratospheric ozone depletion, but also compounds crucial to understanding tropospheric pollution and transport (e.g. CO, C$_2$H$_6$, and HCN).

CO and C$_2$H$_6$ are among the most abundant ozone precursors in the troposphere and play a crucial role in controlling its oxidizing capacity. They are emitted primarily by anthropogenic sources and their main sinks in the troposphere are through reaction with the hydroxyl radical (OH) (e.g. Levy II, 1971). The lifetimes of both species are rather long (50–60 days) (Hough, 1991; Holloway et al., 2000; Rudolph, 1995) and so they are influenced by vertical mixing and long-range transport. This makes them suitable indicators for transport of air pollutants. Biomass burning emissions are the main direct sources of both CO and C$_2$H$_6$ in the Southern Hemisphere (Watson et al., 1990; Fishman et al., 1991; Rinsland et al., 1998; Matsueda et al., 1999). However, in the case of both CO and C$_2$H$_6$, the inter-hemispheric transport of industrial sources from the Northern Hemisphere (NH) to the SH is an important source in the SH, adding to SH biomass-burning sources (e.g. Xiao et al., 2008). For HCN, it is well established that biomass burning is the major source (Lobert et al., 1990; Li et al., 2000, 2003; Singh et al., 2003); however, its sinks are not well quantified. It has a lifetime of around 2–4 months with the main sink suggested to be uptake by the ocean (Li et al., 2000). Therefore, measurements of these species made in the clean SH at mid- to high latitudes are particularly useful in interpreting influences from the southern tropical and sub-tropical biomass burning through long-range transport, as well as in assessing the effect of inter-hemispheric transport of air pollutants from the NH to the SH. (For example, C$_2$H$_6$ has a large global industrial source).

Time series of CO, C$_2$H$_6$ and HCN columns at Lauder measured from the FTIR have been reported previously for various periods (e.g. Rinsland et al., 1998, 2002; Jones et al., 2001; de Laat et al., 2010). Rinsland et al. (1998) showed significant year-to-year variations in both CO and C$_2$H$_6$ partial columns (surface to 12 km) measured at Lauder but the trends over the period 1993–1997 for both species are not significant. Rinsland et al. (2002) reported partial columns of the two species for the period of 1993–2000, as well as HCN for 1998–2000, at Lauder; again no significant long-term trends were found for CO and C$_2$H$_6$. However, Rinsland et al. (2002) reported a downward trend for HCN over this very short time period.

In this paper, we report time series of CO, C$_2$H$_6$, and HCN partial columns from the FTIR measurements at Lauder and Arrival Heights from 1997 to 2009. The Arrival Heights time series of C$_2$H$_6$ and HCN have not been presented before. We calculate the trends of these species at both locations based on the 13-yr time series and analyse their seasonal and interannual variability using a chemistry-climate model (CCM). In the following sections, we briefly describe the measurement technique, which has been extensively described before (e.g. Rinsland et al., 1998, 2002), and describe the CCM used for simulations and the comparison between modelled and observed time series of CO, C$_2$H$_6$ and HCN. Furthermore, we assess the main processes that contribute to the trend and the seasonal and interannual variations of these species at the two stations.

2 Description of measurements and model simulations

The measurement sites are both part of the Network for the Detection of Atmospheric Composition Change (NDACC) (http://www.ndsc.ncep.noaa.gov/). Measurements are possible only on clear days and, at Arrival Heights, there is a period of 4–5 months of polar night each year when solar measurements are not possible. The measurements were made at Arrival Heights with a Bruker model 120M Fourier Transform Spectrometer. The measurements at Lauder were initially made with a similar 120M but were changed to a 120HR Bruker model in September 2001. Both instrument models have the same maximum path difference of 257 cm, resulting in a spectral resolution of 0.0035 cm^{-1}. Mirror tracking systems were used to record direct sun spectra in the mid-infrared (2–14 μm). The retrieval of trace gas information from these recorded spectra was performed using version 3.93 of the profile retrieval algorithm SFIT2 and is similar to that described by Rinsland et al. (1998, 2002) and Morgenstern et al. (2012).

The tropospheric chemistry-climate model, UM-CAM, is used to perform the simulations. The model was evaluated and used in a number of previous studies (e.g. Zeng et al., 2008, 2010; Morgenstern et al., 2012), and is based on the UK Met Office Unified Model version 4.5 (atmosphere only) coupled with a detailed tropospheric chemistry scheme. It has 19 levels from the surface to 4.6 hPa with 6 levels above 150 hPa. Its horizontal resolution is 3.75° by 2.5°. The model uses prescribed sea surface conditions following the Atmospheric Model Intercomparison Project (AMIP) II (http://www-pcmdi.llnl.gov). The chemistry module includes gas phase reactions describing O$_3$-NO$_x$-VOC (volatile organic compound) chemistry, dry and wet deposition, and tabulated photolysis rates as described by Zeng et al. (2008). Daily concentrations of NO$_y$ above 50 hPa are prescribed using the output from a 2-D model (Law and Pyle, 1993). We also prescribe stratospheric ozone with a present-day ozone climatology that is for use in the upcoming Fifth Assessment Report

of Intergovernmental Panel on Climate Change (IPCC AR5) simulations (Cionni et al., 2011). The UM-CAM ozone fields are overwritten in the model domains above 50 hPa between 60° S–60° N and above 100 hPa poleward of ±60°. As the model is not nudged towards observations, its day-to-day variations do not follow the observed weather. However, the seasonal-scale variability in the biomass burning emissions is captured, as well as major meteorological features such as El Niño Southern Oscillation (ENSO) which are present in the ocean-surface forcing.

We include surface emissions of nitrogen oxides (NO_x), CO, C_2H_6, propane (C_3H_8), formaldehyde (HCHO), acetaldehyde (CH_3CHO), acetone (CH_3COCH_3), and isoprene, as well as NO emissions from aircraft in the model. We also include lightning-produced NO_x emissions that are calculated online as a function of model-calculated cloud top height, as described by Zeng et al. (2008) and references therein. The methane mixing ratio is kept as a global constant that is appropriate for year 2000 value, i.e. 1760 ppbv (taken as the average CH_4 mixing ratio during 1995–2005, as given by IPCC (2007)) to minimize the spin-up time of the simulations. For biomass burning emissions, we use the interannually varying Global Fire Emissions Database version 3 (GFED3) covering the years 1997 to 2009 (van der Werf et al., 2010). The industrial sources of the species are adopted from the newly released emission scenarios for IPCC AR5 (Lamarque et al., 2010) for year 2000 conditions. The total emissions of NMVOCs (excluding isoprene) from Lamarque et al. (2010) are partitioned among C_2H_6, C_3H_8, HCHO, CH_3CHO and CH_3COCH_3 in the model to account for the effect of NMVOCs that the model does not include. However, we do not lump any other species' emissions into the C_2H_6 emissions so that the model produces realistic C_2H_6 concentrations. For C_2H_6, we adopt annual emissions of 6.1 Tg from the industrial sources and 1.5–3.0 Tg from biomass burning which is comparable to the annual emission of 8.2 Tg from the EDGAR database (Olivier et al., 1996). We scale the total isoprene emissions from 560 Tg yr^{-1} (Guenther et al., 1995), as used by Zeng et al. (2008) to 390 Tg yr^{-1} in this study; this produces a better match of modelled and measured CO columns, and is close to the estimates of Müller et al. (2008). There are large uncertainties in estimating global total annual isoprene emissions and the implementation of isoprene emissions in global models (Holloway et al., 2000; Duncan et al., 2007; Arneth et al., 2011). To simulate HCN, we only include biomass burning sources that are scaled from the GFED3 (van der Werf et al., 2010) CO biomass burning emissions assuming a single ratio of 0.0057 (HCN/CO) used for all burning types; this ratio is in agreement with the recent compilation of Akagi et al. (2011). Loss of HCN occurs through reaction with OH (the pressure-dependent rate coefficient of Kleinböhl et al. (2006) is used here) and through dry deposition over open water, assuming a deposition velocity of 0.13 cm s^{-1} as given by Li et al. (2000). The global annual biomass-burning emis-
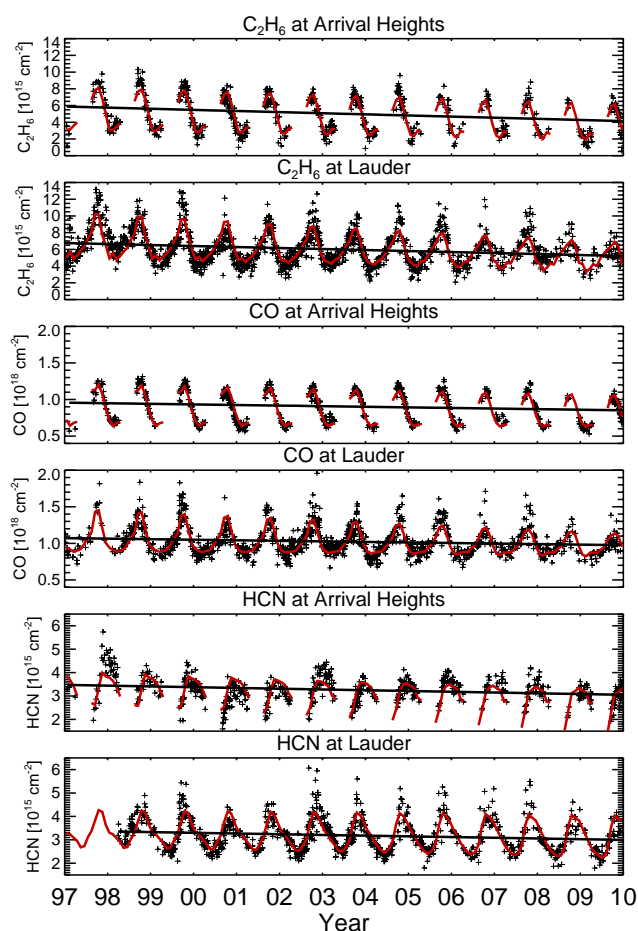
Table 1. Summary of annual total emissions.

	A	B
CO (Tg CO)		
Industrial sources	600	697 (*1997*)–512 (*2009*)
Biomass burning	253–598	253–483
Ocean/vegetation	100	100
NO_x (Tg N)		
Industrial sources	31.6	31.6
Biomass burning	7.4–12.5	7.4–12.5
Soil	7.0	7.0
Aircraft	0.79	0.79
Lightning	4.0	4.0
C_2H_6 (Tg C_2H_6)		
Industrial sources	6.1	8.00 (*1997*)–5.17 (*2009*)
Biomass burning	1.5–3.0	
NMVOCs (Tg VOC)		
Industrial sources	127	127
Biomass burning	15.2–30.2	15.2–30.2
Isoprene	390	390
CH_4 (ppbv)	1760	1760
HCN (Tg HCN)		
Biomass burning	1.45–3.43	1.45–3.43

sions of HCN vary between 1.45 and 3.43 Tg (HCN) yr^{-1}. These numbers are similar to those given by Li et al. (2000) and Lupu et al. (2009). Other sources (e.g. industrial) and loss channels (e.g. via photolysis and through reaction with O(^{1}D)) are minor (Li et al., 2000; Kleinböhl et al., 2006) and therefore are not considered in the simulation here. We summarise the annual total emissions in Table 1.

In simulation A, only biomass burning emissions have year-to-year variations. In simulation B, we use variable industrial emissions of CO and C_2H_6. Here, the emissions are modified from those used in simulation A by imposing linear trends over the period of 1997 to 2009. We also perform simulations using annually periodic biomass burning emission (namely the GFED3 dataset averaged over 1997 to 2009) to contrast simulations A and B and investigate the effect of biomass burning on interannual variations of these species.

3 Observed trends and seasonal and interannual variations in CO, C_2H_6, and HCN partial columns

Figure 1 shows observed daily mean partial columns of CO, C_2H_6, and HCN at Lauder and Arrival Heights (integrated below 12 km), displayed in black symbols. The partial columns of all three species show distinct seasonal cycles with low values during February–April and peaks

Fig. 1. Time series of CO, C_2H_6, and HCN partial columns (molecules cm^{-2}) recorded at Lauder and Arrival Heights (black symbols), month-by-month linear regression (red line) and the multi-annual linear trends (black line).

Table 2. Summary of trends and 2σ uncertainties of CO, C_2H_6, and HCN partial columns at Lauder and Arrival Heights for various periods. Units are in % yr^{-1}.

|	1997–2009	1998–2009	1999–2009
CO Lauder	-0.94 ± 0.47	-0.95 ± 0.48	-0.87 ± 0.43
CO Arrival Heights	-0.92 ± 0.46	-0.89 ± 0.44	-0.72 ± 0.36
C_2H_6 Lauder	-2.37 ± 1.18	-2.07 ± 1.04	-1.42 ± 0.68
C_2H_6 Arrival Heights	-2.82 ± 1.37	-2.67 ± 1.31	-2.30 ± 1.15
HCN Lauder		-0.95 ± 0.47	-0.62 ± 0.31
HCN Arrival Heights	-1.41 ± 0.71	-1.23 ± 0.62	-0.75 ± 0.38

month linear regression. In a separate calculation, we also calculate multi-annual trends by subtracting the mean annual cycle and calculating a linear trend from the remainder, following Rinsland et al. (2002) and Morgenstern et al. (2012). This analysis gives regression coefficients A_0 (a constant offset) and A_1, a linear trend term, and A_1/A_0 is the relative trend discussed below.

The multi-annual relative trends and the uncertainties of daily mean partial columns for all three species are summarised in Table 2. For the period of 1997 to 2009, the trends for the partial columns of CO are -0.94 ± 0.47 % yr^{-1} at Lauder and -0.92 ± 0.46 % yr^{-1} at Arrival Heights. For C_2H_6, the calculated trends are -2.37 ± 1.18 % yr^{-1} at Lauder and -2.82 ± 1.37 % yr^{-1} at Arrival Heights. For HCN, the time series starts in 1998 at Lauder and we calculate -0.95 ± 0.47 % yr^{-1} at Lauder and -1.41 ± 0.71 % yr^{-1} at Arrival Heights. We also calculated the trends over the periods of 1998–2009 and 1999–2009 for comparison, to exclude the ENSO anomaly at the beginning of the time series (see Table 2). Indeed, there are some reductions of the trends in absolute terms for all species at both locations but they remain significant. Note the substantially larger relative trends of C_2H_6 than those of CO and HCN at both locations. Such larger trends of C_2H_6 relative to those of CO have also been detected at Northern Hemisphere locations (e.g. Angelbratt et al., 2011). Aydin et al. (2011) attribute the decline in global C_2H_6 levels since the 1980s to the decrease in emissions of this gas from natural gas production. They also speculate that atmospheric levels of chlorine atoms (Cl*) might have increased which could potentially contribute significantly to the C_2H_6 decline. However, the magnitude of this sink is not well known. Measurements at Wollongong, Australia, also show negative trends of C_2H_6 (C. Paton-Walsh, personal communication, 2011). For C_2H_6, the main processes determining its abundance are its primary emission sources (70 % from emissions associated with natural gas industry, primarily in the NH, and the remainder from biomass burning) and its principal atmospheric sinks through the reaction with OH. Therefore, understanding both the changes in its primary sources and the changes of OH in the past two decades is crucial to understanding its long-term trends. Changes in OH could play a critical role in controlling trends in C_2H_6 in

over August–November at both locations. This indicates that biomass burning in the southern tropics and sub-tropics is the main factor shaping the annual cycle (e.g. Rinsland et al., 1998; Matsueda et al., 1999). The annual cycle and variability of C_2H_6, CO, and HCN partial columns are all larger at Lauder than at Arrival Heights (Morgenstern et al., 2012), presumably due to the larger transport times between the source regions and Arrival Heights, i.e. Antarctic air has experienced more mixing and photochemical removal than air above Lauder.

We form linear trends for each month separately. To account for different measurement densities, for every month covered by the time series, we perform a linear regression through the measurements taken during this month, and then evaluate the linear regression at the middle of the month to define one representative data point for each month. The multi-annual trend is then calculated in a second step by linearly regressing through the representative mid-month values of each month. The result is referred to as the month-by-

this clean environment but recent studies suggest that such changes are likely very small (e.g. Montzka et al., 2011). We examine the interannual variability (IAV) of OH expressed in terms of the methyl chloroform lifetime due to OH loss in the model (which averages to 6.7 yr) and calculate the mean standard deviation of the IAV as 2.7 % between 1997–2009 (with a relatively large variation in 1997–1998). The calculated trend in methyl chloroform lifetime is close to zero over this period. This is in agreement with the IAV of global mean OH inferred from methyl chloroform measurements between 1998 and 2007 (Montzka et al., 2011). By comparison, sources of CO not only comprise direct primary emissions (40–50 %) but also indirect sources from photochemical production (i.e. oxidation of methane and NMVOCs). Of the direct emissions of CO, about 50 % is from industrial sources (see e.g. Horowitz et al., 2003; Duncan et al., 2007). Hence, the contribution from the inter-hemispheric transport of NH industrial sources will be comparatively smaller to SH CO than to SH C$_2$H$_6$. For HCN, the main source is biomass burning and the main sink is ocean dry deposition (Li et al., 2000); either or both of these should be the driving factors of the observed significant negative trends of HCN partial columns at both locations. In Sect. 4 we assess these processes in more detail using the CCM.

Rinsland et al. (2002) found no significant trends for either CO or C$_2$H$_6$ at Lauder between 1994 and 2000, but then these periods are very short for establishing significant trends. The 1997–1998 ENSO has influenced trends over that period, both directly by affecting transport and meteorology, and indirectly by causing major fires in Indonesia (Matsueda et al., 1999). However, Rinsland et al. (2002) report a large negative trend for HCN partial columns at Lauder for 1998–2000 (-8.06 ± 1.06 % yr^{-1}), presumably due to the 1997–1998 ENSO at the beginning of the time series. Here the calculated annual relative trend of HCN partial columns at Lauder from 1998 (the beginning of the HCN time series at this location) to 2009 is -0.95 ± 0.47 % yr^{-1} and the trend is reduced to -0.62 ± 0.31 % yr^{-1} when calculated over the period of 1999 to 2009 (see Table 2). We note that relative trends in both C$_2$H$_6$ and HCN are moderately larger at Arrival Heights than at Lauder. Although the relative trends are not significantly different at a 95 % confidence level, this might indicate a systematic impact of transport or oxidizing capacity changes associated with climate and composition changes, and continued operation of observational platforms will be needed to detect such changes.

Seasonal trends for the three species are exclusively negative (Fig. 2). The monthly trends from August to November are distinctly larger, in absolute terms, than at other months for both C$_2$H$_6$ and CO partial columns at Lauder. This period is the southern tropical biomass burning period and may imply a trend in tropical biomass burning. At Arrival Heights, C$_2$H$_6$ and CO also exhibit larger negative trends over August to November than other months. Note that the large negative trend for C$_2$H$_6$ partial columns in February at Lauder
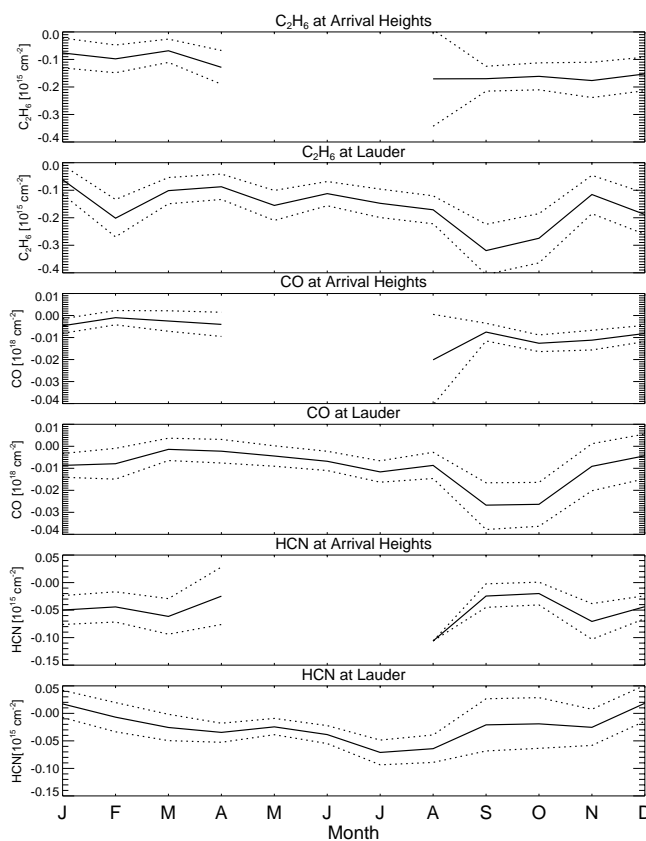
Fig. 2. Month-by-month trends (molecules cm^{-2} yr^{-1}) with associated 95 % confidence limits.

is caused by persistent high levels recorded during February 1997, the beginning of the time series; this substantially affects the seasonal trend (the February trend is reduced from 0.2×10^{15} to 0.12×10^{15} cm^{-2} yr^{-1} when calculated from February 1998). However, the anomaly does not play a significant role in determining the annual trend for the whole period of 1997–2009. For HCN, the negative trends between June and August are relatively larger than for other months at Lauder while at Arrival Height the trends are larger than at Lauder for most of the months.

Figure 3 shows the correlation between the partial columns of CO and C$_2$H$_6$, as well as CO and HCN in the four seasons for Lauder. The correlation coefficients vary with season for both sets of data, and the strongest correlation occurs during September–November when southern tropical biomass burning peaks (i.e. correlation coefficients $r = 0.91$ for CO/C$_2$H$_6$ and $r = 0.86$ for CO/HCN). There are also sizeable correlations between CO and C$_2$H$_6$ during the other seasons ($r = 0.50$ to 0.75). The correlation between CO and HCN is smallest during March–May ($r = 0.47$) when there is almost no southern sub-tropical biomass burning.
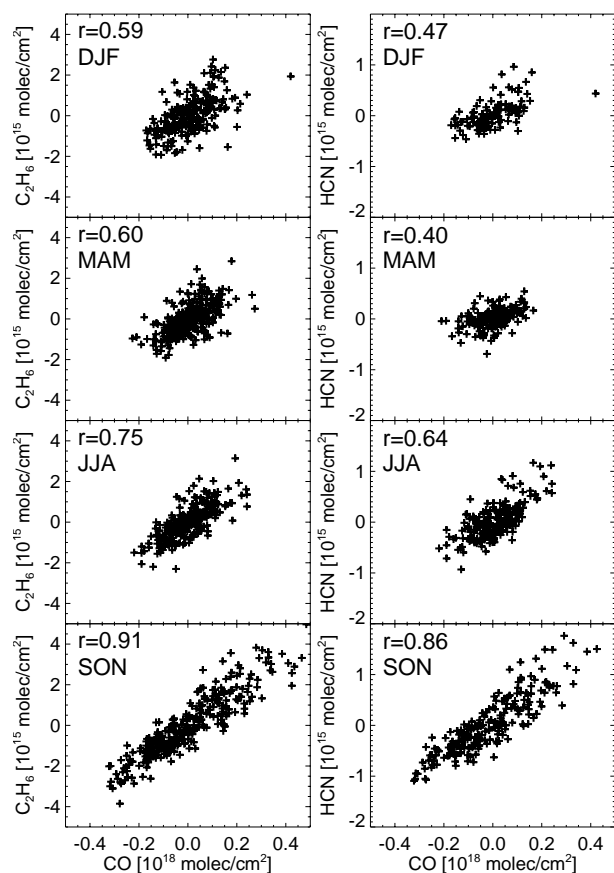
Fig. 3. Tracer-tracer correlative scatter plots for C$_2$H$_6$ and CO, and for HCN and CO, respectively, at Lauder for the four seasons. r indicates Pearson's correlation coefficient. All variables have been deseasonalized and detrended.

4 Comparisons between modelled and observed CO, C$_2$H$_6$, and HCN partial columns

The seasonal and interannual variations of these species are compared with simulations from the UM-CAM CCM described in Sect. 2. Here we apply the a priori and averaging kernels used in the data retrievals to model data when comparing modelled and observed partial columns. The model data are interpolated to the FTIR data levels (which are spaced by 2 km) and time points (for instantaneous data points) and are convolved with the respective a priori and averaging kernel data. We then calculate the differences between modelled and observed data and the corresponding trends of these residuals.

4.1 C$_2$H$_6$

Figure 4 shows observed and modelled (both original and convolved) C$_2$H$_6$ partial columns and the difference between convolved model data minus observations at Lauder and Arrival Heights, for simulations A and B. There is an offset between the convolved and the original model data.

This shows that application of averaging kernels and a-priori data can introduce a bias into observed data in the case of C$_2$H$_6$ columns. However, the correlation between these two datasets is very high ($r = 0.98$ to 0.99). The seasonal cycles are well reproduced by the model and clearly follow the cycle of the southern tropical biomass burning that peaks in austral spring (Hao and Liu, 1994). At Lauder, the observed C$_2$H$_6$ partial columns have larger variability in the observations than in the model. Note that individual and extreme events are generally not captured by the model, and the likely reasons for this include insufficiently variable emissions, excessive model diffusivity, and the coarse model resolution. At Arrival Heights, however, the model data are much smoother owing to the longer transport distance from the emission source regions. The model underestimates the amplitude of the observed C$_2$H$_6$ annual cycles at Arrival Heights to some degree. We also show the original modelled data over wintertime at Arrival Heights when there are no measurements available.

In Fig. 4, the residuals (modelled – observed C$_2$H$_6$) show large trends at both locations (see Table 3) for simulation A with only interannually varying biomass burning emissions in the model. We then perform simulation B with a 35 % decline in global industrial (i.e. fossil fuel and biofuel) emissions of C$_2$H$_6$. Simulation B produces substantially reduced trends of the residuals at both locations (from 2.67 ± 0.19 to 0.72 ± 0.20 at Lauder and from 2.47 ± 0.35 % yr^{-1} to 0.08 ± 0.35 % yr^{-1} at Arrival Heights – see Table 3). We also calculate these trends over 1998–2009 to exclude the anomaly at the begining of the time series and the trends become insignificant (-0.12 ± 0.21 % yr^{-1} at Lauder and -0.12 ± 0.37 % yr^{-1} at Arrival Heights). This shows the important contribution of NH industrial sources to SH C$_2$H$_6$ through inter-hemispheric transport (Xiao et al., 2008); these NH emission trends control the SH C$_2$H$_6$ trends. We carry out additional simulations (assuming a C$_2$H$_6$ tracer with only industrial emissions but with the same loss as "normal" C$_2$H$_6$) and calculate an average of 77 % contribution of global industrial sources to Lauder C$_2$H$_6$ partial columns and an average of 72 % to Arrival Heights C$_2$H$_6$ partial columns. We also calculate separate contributions from NH C$_2$H$_6$ industrial sources to C$_2$H$_6$ partial columns at both locations; an average of 60 % contribution is calculated for Lauder and an average of 50 % for Arrival Heights. (In the emission scenario used here 89 % of global industrial emissions occur in the NH).

4.2 CO

Comparisons between observed and modelled CO are shown in Fig. 5. There is no visible difference between model data with and without averaging kernels applied, and the correlations between the two datasets are close to unity (as also found by Morgenstern et al., 2012). Again the seasonal cycles of observed CO partial columns are well reproduced
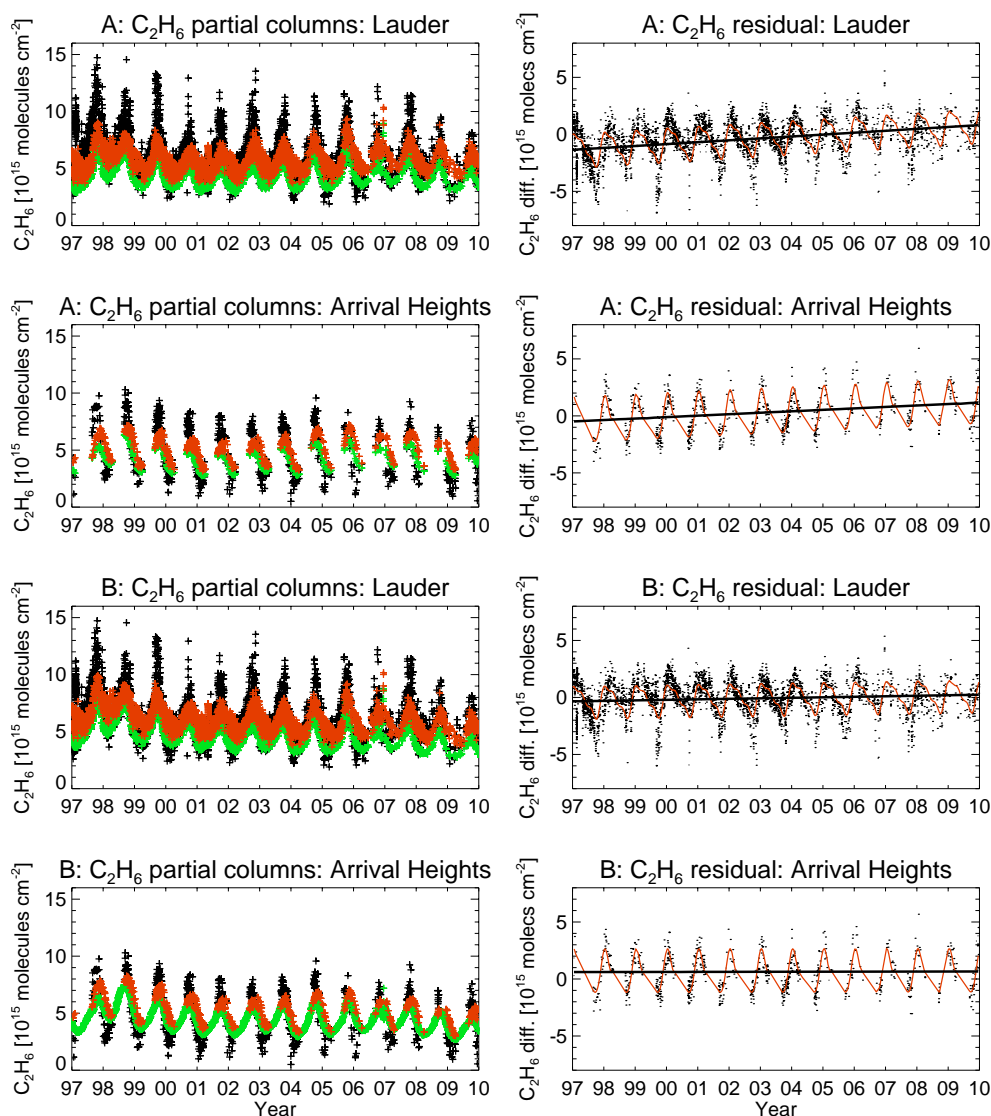
Fig. 4. Left panel: C$_2$H$_6$ partial columns from observed (black), original model (green), and model data convolved with averaging kernels and a priori (red) at Lauder and Arrival Heights. "A" denotes runs with annually periodic anthropogenic emissions and "B" denotes runs with declining anthropogenic emissions in CO and C$_2$H$_6$. Original model data are also shown at Arrival Heights for the wintertime when no measurements were taken (Simulation B). Right panel: corresponding residuals between observed and convolved model data (modelled–observed) for C$_2$H$_6$ at Lauder and Arrivals Heights from runs A and B. Black symbols denote observed residuals, red lines denote 4th order trigonometric-polynomials and a linear trend regression fitted to the residuals, and black lines are only the linear trends of those regression functions.

by the model, and the minima from March to June and the maxima from August to November show that the seasonal cycle is largely determined by southern tropical and sub-tropical biomass burning (Rinsland et al., 2002). The wintertime modelled CO columns are also shown at Arrival Heights. Note that modelled CO at Arrival Heights is slightly higher than the observed CO for the minima values and this is clearly shown in residuals between modelled and observed data.

The residuals (modelled–observed) calculated from simulations with only interannually varying biomass burning emissions show upward trends for CO at Lauder (0.88 ± 0.17 % yr^{-1}) and Arrival Heights (0.61 ± 0.15 % yr^{-1}) which are moderate reductions compared with simulation C with periodic emissions from all sources (see Fig. 5 and Table 3). When applying a 26 % decline of CO industrial emissions from 1997 to 2009, we find that the trends of the residuals reduce to 0.13 ± 0.17 % yr^{-1} and −0.10 ± 0.14 % yr^{-1} at Lauder and Arrival Heights, respectively; these trends are insignificant. This suggests that industrial sources are also a significant factor in determining CO trends in the SH.

Table 3. Trends of the residuals and 2σ uncertainties from the run with interannually varying biomass burning emissions and non-varying industrial emissions (A), the run with interannually varying biomass burning emissions and decling anthropogenic emissions of C$_2$H$_6$ and CO (B), and the run with annually periodic biomass burning and anthropogenic emissions (C) over the period of 1997–2009: modelled-observed. Units are in % yr^{-1} relative to the mean partial columns of the observed FTIR data. Values in italics denote trends calculated from 1998.

| | Lauder | | | Arrival Heights | | |
	A	B	C	A	B	C
C$_2$H$_6$	2.67 ± 0.19	0.72 ± 0.20	2.88 ± 0.21	2.47 ± 0.35	0.08 ± 0.35	2.92 ± 0.38
C$_2$H$_6$ *(1998–2009)*	*1.93 ± 0.21*	*−0.12 ± 0.21*	*2.47 ± 0.24*	*2.27 ± 0.37*	*−0.12 ± 0.37*	*2.69 ± 0.39*
CO	0.88 ± 0.17	0.13 ± 0.17	0.91 ± 0.17	0.61 ± 0.15	−0.10 ± 0.14	0.91 ± 0.15
HCN	−0.39 ± 0.23		0.93 ± 0.22	0.31 ± 0.30		1.47 ± 0.29
HCN *(April 1998–2009)*	*−0.11 ± 0.22*			*0.08 ± 0.22*		
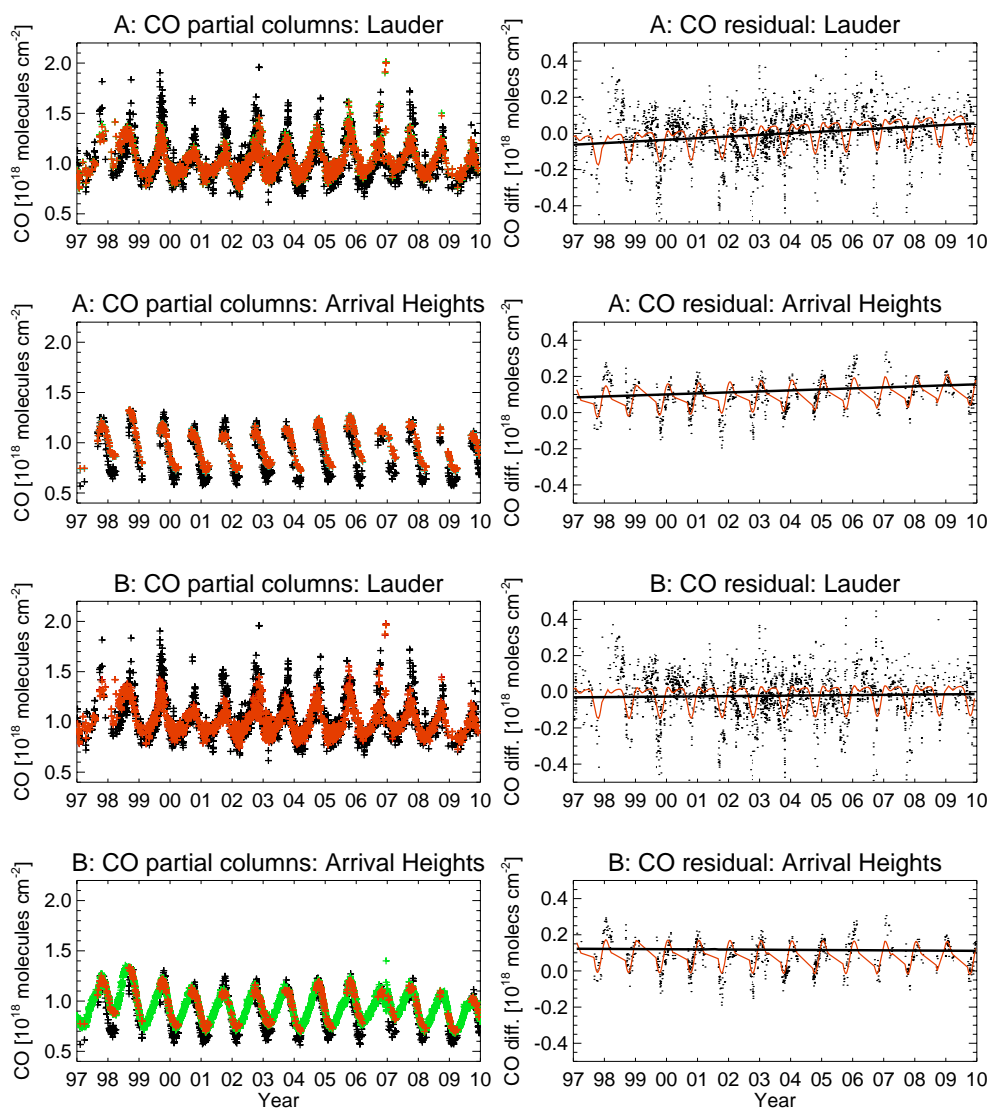
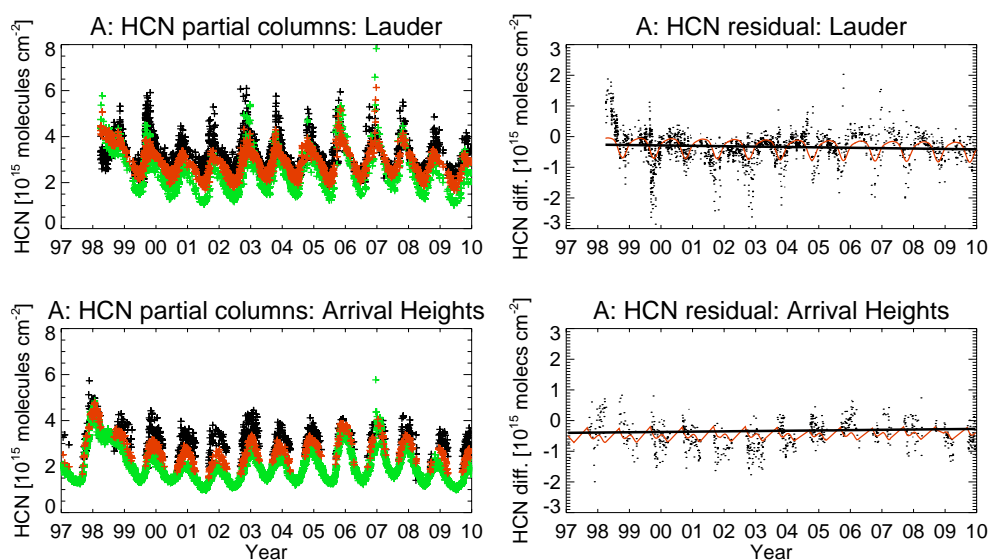**Fig. 5.** Same as Fig. 4 but for CO.

Fig. 6. Same as Fig. 4 for HCN with just simulation A.

To assess the influence of increasing methane on the trends in CO, we have carried out a sensitivity test assuming a 1.7 % increase of global methane during the period of 1997−2009; we calculate a 0.9% increase of CO columns ($0.068\,\%\,\mathrm{yr}^{-1}$) which is substantially smaller than the trends of the CO partial columns at both locations.

4.3 HCN

At both locations, HCN observations are well reproduced by the model (Fig. 6), although the peak values of some years are underestimated by the model, especially at Arrival Heights. This may imply an underestimation of the amplitude of the biomass burning annual cycles in the model. The wintertime HCN columns from the model are shown. There are clear differences between the original and the convolved model data but the correlation between the two datasets is again very high ($r = 0.98$ to 0.99). We use a retrieval method similar to that described above and the calculated averaging kernels are consistent with those used by Zhao et al. (2002). The amplitudes and the phases of the annual cycles are fairly well reproduced by the model and are consistent with those published by Lupu et al. (2009).

The calculated trends of the residuals (modelled-observed) for HCN at Lauder and at Arrival Heights are $-0.39 \pm 0.23\,\%\,\mathrm{yr}^{-1}$ and $0.31 \pm 0.30\,\%\,\mathrm{yr}^{-1}$ respectively, and are significantly smaller (in absolute terms) than those derived from simulations using biomass burning emissions averaged over 1997–2009 (see Fig. 6 and Table 3). The Lauder HCN time series starts in 1998. At the beginning of the time series the discrepancy between the modelled and observed columns is quite large. Excluding the first 3 months data in 1998, we calculate a residual trend of $-0.11 \pm 0.22\,\%\,\mathrm{yr}^{-1}$; this is statistically insignificant. The same applies to Arrival Heights

(a residual trend of $0.08 \pm 0.22\,\%\,\mathrm{yr}^{-1}$ is calculated for this same period). This is consistent with biomass burning being exclusively responsible for the observed trends of HCN columns at both locations.

4.4 Impact of tropical biomass burning emissions

To examine the effect of biomass burning on the year-to-year variations of CO, C₂H₆, and HCN partial columns, we contrast the model simulation A (interannually varying biomass burning emissions) to the simulation C that uses annually periodic biomass burning emissions. Figure 7 shows the daily mean percentage deviations of CO, C₂H₆, and HCN partial columns due to variations in biomass burning (i.e. $100 \times (A - C)/C$) at Lauder and Arrival Heights. At both stations and for all three species, the most substantial anomaly occurred during the 1997–1998 ENSO event which caused sustained burning in Indonesia. The anomalies at both locations are well correlated, indicating a persistent influence of transport of biomass burning pollutants over a large distance. For all three species, the Lauder signal contains more short-lived spikes than the Arrival Heights series, suggesting either that the short-lived spikes disappear over the typically 2.5 weeks of transport and mixing which separate the two sites (Morgenstern et al., 2012), or possibly that there is an occasional influence of local emissions on the Lauder signal. Relative variations associated with C₂H₆ are larger than CO for both locations, whereas HCN has the largest variations due to variations in biomass burning emissions.

We also assess the impact of biomass burning emissions from different SH tropical and sub-tropical regions on CO partial columns at mid- and high latitudes. We perform four sensitivity simulations which are identical to simulation A but biomass burning emissions from sub-equatorial Africa,
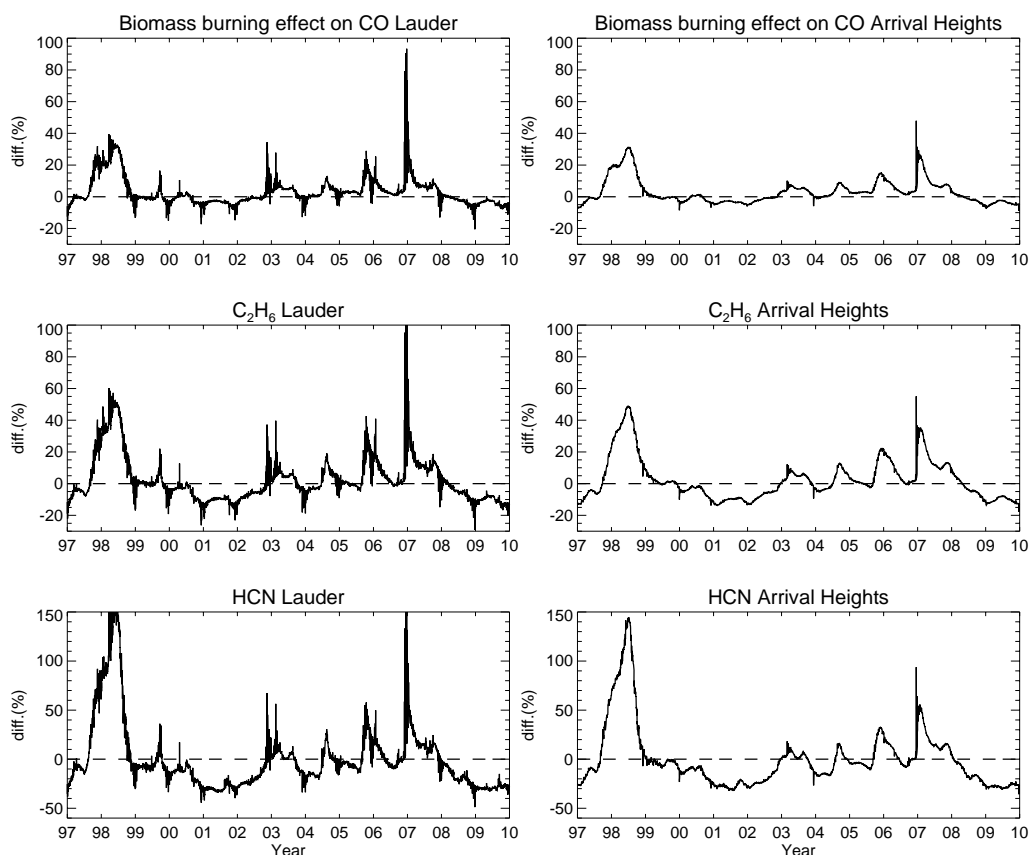
Fig. 7. Percentage differences of CO, C$_2$H$_6$, and HCN partial columns simulated with interannually varying biomass burning emissions, relative to a simulation with annually periodic biomass burning emissions, taken as the average over 1997–2009.

South America, South-East Asia, and Australia, respectively, are reduced by 50 %. Figure 8 shows differences in the CO columns at Lauder and Arrival Heights between the four simulations, relative to the baseline A simulation. The results indicate that African biomass burning dominates the background seasonality of SH CO columns, followed by emissions from South America. For most years, the contributions from South-East Asia and Australia are smaller in comparison, but they dominate the large peaks in 1998 and 2007, presumably as a result of the Indonesian fires in 1998 and Australian bush fires in late 2006 (the Great Divide Fires of 2006–2007 in Victoria). According to our sensitivity simulation, the 2006 Indonesian fires that contributed to elevated CO columns at Darwin (Paton-Walsh et al., 2010) do not have a significant influence on CO columns at Lauder and Arrival Heights. The simulation also indicates that the 2006 peak shown in Fig. 8 is caused by anomalously intensive burning in South America in late 2005.
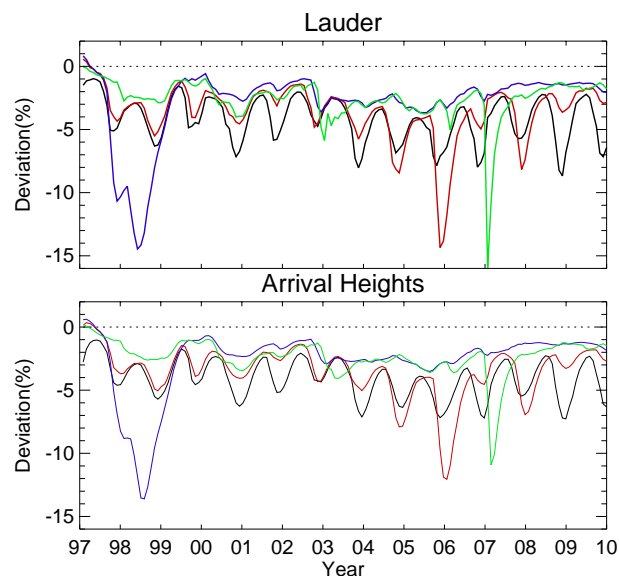
Fig. 8. Percentage differences of CO columns at Lauder and Arrival Heights, caused by 50 % reductions of biomass burning emissions from southern Africa (black), South America (red), South-East Asia (blue), and Australia (green).

5 Conclusions

We have analysed the Lauder and Arrival Heights CO, C$_2$H$_6$, and HCN partial column time series from the FTIR measurements from 1997 to 2009. Statistically, significant negative trends have been recorded for all three species at both locations (ranging from -0.92 to -2.82 % per year). For C$_2$H$_6$ and HCN, relative trends at Arrival Heights are slightly larger than those at Lauder. C$_2$H$_6$ trends are significantly larger than CO and HCN trends at both locations. Maximum absolute trends occur in August to November for CO and C$_2$H$_6$ and June to September for HCN. The model reproduces well the year-to-year variability of CO and C$_2$H$_6$ at both locations but cannot reproduce the long-term trends with simulations that only include interannually varying biomass burning emissions from the GFED3 database. The simulation which assumes a 26 % decline in industrial emissions for CO and a 35 % decline for C$_2$H$_6$ from 1997 to 2009 greatly reduces the differences in modelled and observed trends at both Lauder and Arrival Heights. Modelled HCN partial columns well reproduce both the seasonal cycle and the trends of observed HCN at both locations using interannually varying biomass burning emissions. Driven with only annually periodic biomass burning emissions, the model does not capture the negative trends of observed HCN at either location.

CO and C$_2$H$_6$, and CO and HCN partial columns are highly correlated, particularly during austral spring which is the primary SH tropical biomass burning season. All three species have similar seasonal variations peaking in austral spring. Larger year-to-year variability is observed at Lauder, compared to Arrival Heights. This variability is largely caused by variations in SH tropical biomass burning. Model simulations indicate that biomass burning in southern Africa and South America contributes substantially to the background seasonal variations of CO at Lauder and Arrival Heights. However, Indonesian fires triggered by the 1997–1998 ENSO and the prolonged 2006 Australian bush fires cause peaks in CO columns observed at Lauder for these periods. These peaks propagate efficiently to high latitudes.

References

Akagi, S. K., Yokelson, R. J., Wiedinmyer, C., Alvarado, M. J., Reid, J. S., Karl, T., Crounse, J. D., and Wennberg, P. O.: Emission factors for open and domestic biomass burning for use in atmospheric models, Atmos. Chem. Phys., 11, 4039–4072, doi:10.5194/acp-11-4039-2011, 2011.

Angelbratt, J., Mellqvist, J., Simpson, D., Jonson, J. E., Blumenstock, T., Borsdorff, T., Duchatelet, P., Forster, F., Hase, F., Mahieu, E., De Mazière, M., Notholt, J., Petersen, A. K., Raffalski, U., Servais, C., Sussmann, R., Warneke, T., and Vigouroux, C.: Carbon monoxide (CO) and ethane (C$_2$H$_6$) trends from ground-based solar FTIR measurements at six European stations, comparison and sensitivity analysis with the EMEP model, Atmos. Chem. Phys., 11, 9253–9269, doi:10.5194/acp-11-9253-2011, 2011.

Arneth, A., Schurgers, G., Lathiere, J., Duhl, T., Beerling, D. J., Hewitt, C. N., Martin, M., and Guenther, A.: Global terrestrial isoprene emission models: sensitivity to variability in climate and vegetation, Atmos. Chem. Phys., 11, 8037–8052, doi:10.5194/acp-11-8037-2011, 2011.

Aydin, M., Verhulst, K. R., Saltzman, E. S., Battle, M. O., Montzka, S. A., Blake, D. R., Tang, Q., and Prather, M. J.: Recent decreases in fossil-fuel emissions of ethane and methane derived from firn air, Nature, 476, 198–201, 2011.

Cionni, I., Eyring, V., Lamarque, J. F., Randel, W. J., Stevenson, D. S., Wu, F., Bodeker, G. E., Shepherd, T. G., Shindell, D. T., and Waugh, D. W.: Ozone database in support of CMIP5 simulations: results and corresponding radiative forcing, Atmos. Chem. Phys., 11, 11267–11292, doi:10.5194/acp-11-11267-2011, 2011.

de Laat, A. T. J., Gloudemans, A. M. S., Schrijver, H., Aben, I., Nagahama, Y., Suzuki, K., Mahieu, E., Jones, N. B., Paton-Walsh, C., Deutscher, N. M., Griffith, D. W. T., De Mazière, M., Mittermeier, R. L., Fast, H., Notholt, J., Palm, M., Hawat, T., Blumenstock, T., Hase, F., Schneider, M., Rinsland, C., Dzhola, A. V., Grechko, E. I., Poberovskii, A. M., Makarova, M. V., Mellqvist, J., Strandberg, A., Sussmann, R., Borsdorff, T., and Rettinger, M.: Validation of five years (2003–2007) of SCIAMACHY CO total column measurements using ground-based spectrometer observations, Atmos. Meas. Tech., 3, 1457–1471, doi:10.5194/amt-3-1457-2010, 2010.

Duncan, B. N., Logan, J. A., Bey, I., Megretskaia, I. A., Yantosca, R. M., Novelli, P. C., Jones, N. B., and Rinsland, C. P.: Global budget of CO, 1988–1997: Source estimates and validation with a global model, J. Geophys. Res., 112, D22301, doi:10.1029/2007JD008459, 2007.

Fishman, J., Fakhruzzaman, K., Cros, B., and Nganga, D.: Identification of widespread pollution in the southern hemisphere deduced from satellite analyses, Science, 252, 1693–1696, 1991.

Guenther, A., Hewitt, C. N., Erickson, D., Fall, R., Geron, C., Graedel, T., Harley, P., Klinger, L., Lerdau, M., Mckay, W. A., Pierce, T., Scholes, B., Steinbrecher, R., Tallamraju, R., Taylor, J., and Zimmerman, P.: A global model of natural volatile organic compound emissions, J. Geophys. Res., 100, 8873–8892, 1995.

Hao, W. M. and Liu, M.-H.: Spatial and temporal distribution of tropical biomass burning, Global Biogeochem. Cy., 8, 495–503, 1994.

Holloway, T., Levy II, H., and Kasibhatla, P.: Global distribution of carbon monoxide, J. Geophys. Res., 105, 12123–12147, doi:10.1029/1999JD901173, 2000.

Horowitz, L. W., Walters, S., Mauzerall, D. L., Emmons, L. K., Rasch, P. J., Granier, C., Tie, X., Lamarque, J.-F., Schultz, M. G., Tyndall, G. S., Orlando, J. J., and Brasseur, G. P.: A global simulation of tropospheric ozone and related tracers: Description and evaluation of MOZART, version 2, J. Geophys. Res., 108, 4784, doi:10.1029/2002JD002853, 2003.

Hough, A. M.: Development of a two-dimensional global tropospheric model: Model chemistry, J. Geophys. Res., 96, 7325–7362, 1991.

IPCC: Climate Change 2007: The Physical Science Basis. Contribution of Working Group I to the Fourth Assessment Report of the Intergovernmental Panel on Climate Change, edited by: Solomon, S., Qin, D., Manning, M., Chen, Z., Marquis, M., Averyt, K. B., Tignor, M., and Miller, H. L., Cambridge Univ. Press, Cambridge, United Kingdom and New York, NY, USA, 996 pp., 2007.

Jones, N. B., Rinsland, C. P., Liley, J. B., and Rosen, J.: Correlation of aerosol and carbon monoxide at 45° S: Evidence of biomass burning emissions, Geophys. Res. Lett., 28, 709–712, 2001.

Kleinböhl, A., Toon, G. C., Sen, B., Blavier, J.-F. L., Weisenstein, D. K., Strekowski, R. S., Nicovich, J. M., Wine, P. H., and Wennberg, P. O.: On the stratospheric chemistry of hydrogen cyanide, Geophys. Res. Lett., 33, L11806, doi:10.1029/2006GL026015, 2006.

Lamarque, J.-F., Bond, T. C., Eyring, V., Granier, C., Heil, A., Klimont, Z., Lee, D., Liousse, C., Mieville, A., Owen, B., Schultz, M. G., Shindell, D., Smith, S. J., Stehfest, E., Van Aardenne, J., Cooper, O. R., Kainuma, M., Mahowald, N., McConnell, J. R., Naik, V., Riahi, K., and van Vuuren, D. P.: Historical (1850–2000) gridded anthropogenic and biomass burning emissions of reactive gases and aerosols: methodology and application, Atmos. Chem. Phys., 10, 7017–7039, doi:10.5194/acp-10-7017-2010, 2010.

Law, C. S. and Pyle, J. A.: Modelling trace gas budgets in the troposphere: 1. Ozone and odd nitrogen, J. Geophys. Res., 98, 18377–18400, 1993.

Levy, H., II: Normal atmosphere: Large radical and formaldehyde concentrations predicted, Science, 173, 141–143, 1971.

Li, Q., Jacob, D. J., Bey, I., Yantosca, R. M., Zhao, Y., Kondo, Y., and Notholt, J.: Atmospheric Hydrogen Cyanide (HCN): Biomass Burning Source, Ocean Sink?, Geophys. Res. Lett., 27, 357–360, 2000.

Li, Q., Jacob, D. J., Yantosca, R. M., Heald, C. L., Singh, H. B., Koike, M., Zhao, Y., Sachse, G. W., and Streets, D. G.: A global three-dimensional model analysis of the atmospheric budgets of HCN and CH$_3$CN: Constraints from aircraft and ground measurements, J. Geophys. Res., 108, 8827, doi:10.1029/2002JD003075, 2003.

Lobert, J. M., Scharffe, D. H., Hao, W. M., and Crutzen, P. J.: Importance of biomass burning in the atmospheric budgets of nitrogen-containing gases, Nature, 346, 552–554, 1990.

Lupu, A., Kaminski, J. W., Neary, L., McConnell, J. C., Toyota, K., Rinsland, C. P., Bernath, P. F., Walker, K. A., Boone, C. D., Nagahama, Y., and Suzuki, K.: Hydrogen cyanide in the upper troposphere: GEM-AQ simulation and comparison with ACE-FTS observations, Atmos. Chem. Phys., 9, 4301–4313, doi:10.5194/acp-9-4301-2009, 2009.

Matsueda, H., Inoue, H. Y., Ishii, M., and Tsutsumi, Y.: Large injection of carbon monoxide into the upper troposphere due to intense biomass burning in 1997, J. Geophys. Res., 104, 28867–28879, 1999.

Montzka, S. A., Krol, M., Dlugokencky, E., Hall, B., Jöckel, P., and Lelieveld, J.: Small interannual variability of global atmospheric hydroxyl, Science, 331, 67–69, 2011.

Morgenstern, O., Zeng, G., Wood, S. W., Robinson, J., Smale, D., Paton-Walsh, C., Jones, N. B., and Griffith, D. W. T.: Long-range correlations in Fourier transform infrared, satellite, and modeled CO in the Southern Hemisphere, J. Geophys. Res., 117, D11301, doi:10.1029/2012JD017639, 2012.

Müller, J.-F., Stavrakou, T., Wallens, S., De Smedt, I., Van Roozendael, M., Potosnak, M. J., Rinne, J., Munger, B., Goldstein, A., and Guenther, A. B.: Global isoprene emissions estimated using MEGAN, ECMWF analyses and a detailed canopy environment model, Atmos. Chem. Phys., 8, 1329–1341, doi:10.5194/acp-8-1329-2008, 2008.

Olivier, J. G. J., Bouwman, A. F., van der Maas, C. W. M., Berdowski, J. J. M., Veldt, C., Bloos, J. P. J., Visschedijk, A. J. H., Zandveld, P. Y. J., and Haverlag, J. L.: Description of EDGAR Version 2.0: A Set of Global Emission Inventories of Greenhouse Gases and Ozone-Depleting Substances for All Anthropogenic and Most Natural Sources on a Per Country Basis and on 1° × 1° Grid, 141 pp., Natl. Inst. of Public Health and the Environ., Bilthoven, Netherlands, 1996.

Paton-Walsh, C., Deutscher, N. M., Griffith, D. W. T., Forgan, B. W., Wilson, S. R., Jones, N. B., and Edwards, D. P.: Trace gas emissions from savannah fires in northern Australia, J. Geophys. Res., 115, D16314, doi:10.1029/2009JD013309, 2010.

Rinsland, C. P., Jones, N. B., Connor, B. J., Logan, J. A., Pougatchev, N. S., Goldman, A., Murcray, F. J., Stephen, M., Pine, A. S., Zander, R., Mahieu, E., and Demoulin, P.: Northern and southern hemisphere ground-based infrared spectroscopic measurements of tropospheric carbon monoxide and ethane, J. Geophys. Res., 103, 28197–28217, 1998.

Rinsland, C. P., Jones, N. B., Connor, B. J., Wood, S. W., Goldman, A., Stephen, T. M., Murcray, F. J., Chiou, L. S., Zander, R., and Mahieu, E.: Multiyear infrared solar spectroscopic measurements of HCN, CO, C$_2$H$_6$, and C$_2$H$_2$ tropospheric columns above Lauder, New Zealand (45° S latitude), J. Geophys. Res., 107, D14, doi:10.1029/2001JD001150, 2002.

Rudolph, J.: The tropospheric distribution and budget of ethane, J. Geophys. Res., 100, 11369–11381, 1995.

Singh, H. B., Salas, L., Herlth, D., Kolyer, R., Czech, E., Viezee, W., Li, Q., Jacob, D. J., Blake, D., Sachse, G., Harward, C. N., Fuelberg, H., Kiley, C. M., Zhao, Y., and Kondo, Y.: In situ measurements of HCN and CH$_3$CN over the pacific Ocean: Sources, sinks, and budgets, J. Geophys. Res., 108, 8795, doi:10.1029/2002JD003006, 2003.

van der Werf, G. R., Randerson, J. T., Giglio, L., Collatz, G. J., Mu, M., Kasibhatla, P. S., Morton, D. C., DeFries, R. S., Jin, Y., and van Leeuwen, T. T.: Global fire emissions and the contribution of deforestation, savanna, forest, agricultural, and peat fires (1997–2009), Atmos. Chem. Phys., 10, 11707–11735, doi:10.5194/acp-10-11707-2010, 2010.

Watson, C. E., Fishman, J., and Reichle Jr., H. G.: The significance of biomass burning as a source of carbon monoxide and ozone in the southern hemisphere tropics: A satellite analysis, J. Geophys. Res., 95, 16443–16450, 1990.

Xiao, Y., Logan, J. A., Jacob, D. J., Hudman, R. C., Yantosca, R., and Blake, D. R.: Global budget of ethane and regional constraints on U.S. sources, J. Geophys. Res., 113, D21306, doi:10.1029/2007JD009415, 2008.

Zeng, G., Pyle, J. A., and Young, P. J.: Impact of climate change on tropospheric ozone and its global budgets, Atmos. Chem. Phys., 8, 369–387, doi:10.5194/acp-8-369-2008, 2008.

Zeng, G., Morgenstern O., Braesicke P., and Pyle, J. A.: Impact of stratospheric ozone recovery on tropospheric ozone and its budget, Geophys. Res. Lett., 37, L09805, doi:10.1029/2010GL042812, 2010.

Zhao, Y., Strong, K., Kondo, Y., Koike, M., Matsumi, Y., Irie, H., Rinsland, C. P., Jones, N. B., Suzuki, K., Nakajima, H., Nakane, H., and Murata, I.: Spectroscopic measurements of tropospheric CO, C$_2$H$_6$, C$_2$H$_2$, and HCN in northern Japan, J. Geophys. Res., 107, 4343, doi:10.1029/2001JD000748, 2002.